Astronomy & Astrophysics

Luminosity and mass function of galactic open clusters
I. NGC 4815[*]

L. Prisinzano[1,2], G. Carraro[2], G. Piotto[2], A. F. Seleznev[3], P. B. Stetson[4], and I. Saviane[5]

[1] Osservatorio Astronomico di Palermo, Piazza del Parlamento 1, 90134, Palermo, Italy
[2] Dipartimento di Astronomia, Università di Padova, Vicolo dell'Osservatorio 5, 35122 Padova, Italy
[3] Astronomical Observatory, Ural State University, pr. Lenina 51, Ekaterinburg, 620083 Russia
[4] Dominion Astrophisical Observatory, Herzberg Institute of Astrophysics, National Res earch Council of Canada, 5071 West Saanich Road, Victoria, British Columbia V8X 4M6, Canada
[5] UCLA/ Department of Physics and Astronomy, Los Angeles, CA 90095-1562, USA

Abstract. We present deep V and I photometry for the open cluster NGC 4815 and four surrounding Galactic fields down to a limiting magnitude $V \sim 25$. These data are used to study cluster spatial extension by means of star counts, and to derive the luminosity (LF) and mass function (MF). The radius turns out to be 3.6 ± 0.3 arcmin at $V = 19.0$, whereas the mass is $880 \pm 230\ m_\odot$ down to $V = 20.8$. From the color-magnitude diagram, we obtain the LFs in the V and I bands, using both the standard histogram and an adaptive kernel. After correction for incompleteness and field star contamination, the LFs were transformed into the present day mass functions (PDMF). The PDMFs from the V and I photometry can be represented as a power-law with a slope $\alpha = 3.1 \pm 0.3$ and $\alpha = 2.9 \pm 0.3$ (the (Salpeter 1955) MF in this notation has a slope $\alpha = 2.35$) respectively, in the mass range $2.5 \leq \frac{m}{m_\odot} \leq 0.8$. Below this mass, the MF cannot be considered as representative of the cluster IMF, as it is the result of the combined effect of strong irregularities in the stellar background, probable internal dynamical evolution of the cluster and/or interaction of the cluster with the dense Galactic field. Unresolved binaries and mass segregation can only flatten the apparent derived IMF, so we expect that the real IMF must be steeper than the quoted slope by an unknown amount.

Key words. open clusters and associations; individual: NGC 4815 – methods: statistical

1. Introduction

Galactic open clusters are loose and weakly bound systems, which only in exceptional cases survive more than 10^8 yrs (van den Bergh & McClure 1980). Their mean lifetime is determined by two factors: the birth-place (or the orbit) and the initial mass. The dissolution of open star clusters is mainly due to close encounters with giant molecular clouds which are very frequent in the galactic thin disk (Theuns 1992a; Theuns 1992b). For this reason, the age distribution is strongly biased towards young objects (Wielen 1971). Out of about 1200 open clusters which are known in the thin disk, only 80 are older than the Hyades (Friel 1995).

The dynamical evolution of open star clusters in the Galactic disk environment was studied by several authors (Terlevich 1987; Theuns 1992a; Theuns 1992b) To summarize, it was shown that encounters with dense molecular clouds are catastrophic, whereas diffuse clouds do not completely destroy the cluster. Moreover, tidal effects induced by the general Galactic gravitational field significantly disturb cluster evolution, producing distorted debris, at the center of which a few closely bound stars remain, with a large fraction of binaries.

On the other hand, the internal dynamics of open clusters was investigated by means of N-body models (Aarseth 1996; de la Fuente Marcos 1997), which include the effects of stellar evolution and a fine treatment of binaries and/or multiple stars.

Among others, a very important result is that the cluster evolution crucially depends on the Initial Mass Function (IMF), and on the cluster richness. De la Fuente Marcos (1997) found that power-law (Salpeter 1955) like IMFs accelerate the cluster disruption if the initial population is small, and that at the end of the evolution, a huge number of binary systems with the same mass is formed.

---

[*] Based on observations made at the European Southern Observatory, La Silla, Chile.

An important constraint for all these models is the possibility of deriving the IMF from observations of open star clusters. Unfortunately, this is a very difficult task for several reasons.

First, most open clusters are poorly populated ensembles of stars, containing from tens to hundreds of stars, and only in rare cases up to some thousands. Secondly, they are located in the inner regions of the thin disk. This fact renders it very difficult to detect cluster members (at odds with globular clusters), due to the high contamination of the field stars in the same line of sight as the clusters. Third, they can be strongly obscured due to interstellar absorption lying between us and the cluster (Janes & Adler 1982).

Probably, the most challenging task is to determine cluster membership. This is feasible for objects close to the Sun, for which we can obtain high quality radial velocity and proper motion measurements. Farther away one has to rely on statistical corrections which usually are made by comparing the cluster with the field in its outskirts. Ideally, when a correction for field star contamination was performed, a reasonable actual (Present Day) mass function (PDMF) can be derived from the observed LF. By modeling the dynamical evolution of the cluster, the PDMF can be converted into an IMF which can be compared with the MFs of other clusters to look for similarities or deviations.

In this paper, the first of a series dedicated to obtaining luminosity and mass functions for Galactic open clusters, we present results for NGC 4815, a rather rich, distant open cluster located at about 2.5 kpc from the Sun.

The ultimate goal is to provide a sample of PDMFs as a function of cluster age, population, and location, to serve as template for N-body models.

We plan to study other clusters with the same method in forthcoming papers. In order to obtain a good representation of the field stellar population, in addition to the cluster we observed four nearby Galactic fields, whose population was averaged and used for the statistical subtraction of the foreground/background objects from the cluster. An adaptive kernel estimator was then applied to obtain a continuous LF, free of binning bias, together with the standard histogram technique. Finally, the MF was derived from $m = 4\,m_\odot$ down to $m = 0.35\,m_\odot$ by using the luminosity-mass relation from the Girardi et al. (2000) models.

Section 2 summarizes our present knowledge of the open cluster NGC 4815. In Sect. 3 we present the observations and data reduction technique; Sect. 4 is dedicated to the discussion of the CMDs obtained for the cluster and the field. Section 5 is contains a detailed analysis of the star counts, while Sect. 6 deals with the LFs derived using the two different techniques. Section 7 presents the MF of NGC 4815 and the comparison with other MFs. Section 8 summarizes our results.

Table 1. NGC 4815 fundamental parameters. Age, distance and reddening are taken from the study of Carraro & Ortolani (1994)

l	303.63
b	-2.09
$E(B-V)$	0.70 ± 0.05
$(m-M)_V$	14.10 ± 0.05
$(m-M)_I$	13.20 ± 0.05
Age	$(0.5 \pm 0.25)\,10^9$ yr
Z	≈ 0.008

2. Previous investigations

NGC 4815 was studied in the past by several authors.

The first photometric data were collected by Moffat & Vogt (1973), who studied 9 stars in the cluster region, but did not recognize any sequence.

Kjeldsen & Frandsen (1991) presented a catalogue of UBV photometry for 559 stars.

Carraro & Ortolani (1994) first made an accurate analysis of the CMD by obtaining BV photometry of 2500 stars down to $V = 19.5$. Their results led to the determination of the cluster parameters: NGC 4815 turns out to be of intermediate age (about half a Gyr old, like the Hyades), with a reddening $E(B-V) \approx 0.70$, and a distance of about 2.5 kpc from the Sun. The metallicity is half Solar (see Table 1). From a preliminary analysis of the MS mass function they obtained an index $\alpha = 2.55$, slightly higher than the classical Salpeter value.

These data were used to study the cluster structure and luminosity function with a different method by Chen et al. (1998), who obtained for the first time the cluster mass function by subtracting the field contamination with a Galaxy structure model. In the mass range $1.1 < \frac{m}{m_\odot} < 2.2$ they obtain a slope $\alpha = 1.97 \pm 0.17$, and a total mass of 912 $m_\odot$ to the photometric limit ($V = 19$). They also found evidence for mass segregation.

3. Observations and reduction

3.1. Observations

NGC 4815 was observed with the ESO-NTT telescope on April 14–16, 1999. We used the EMMI red arm, equipped with the 2048×2048 ESO#36 Tektronics CCD. The scale on the sky is 0.27 arcsec/pixel, for a total field of 9.2 × 9.2 arcmin^2. The observing log is given in Table 1. Almost all the images were collected in sub-arcsec seeing conditions and in photometric conditions. During the same nights, four Galactic fields were observed. These fields are located at 30 arcmin from the center of NGC 4815, on the North, South, East and West sides, respectively. The exposure times and the seeing of the Galactic field images are the same as for the cluster data, with the exception of the southern one, for which only short exposures could be obtained. We opted to exclude this field in the statistical analysis of luminosity and mass function.

Table 2. Log-book of the NGC 4815 observations

Field	Filter	Exp. Time [s]	Seeing $FWHM['']$
Center	V	15	0.8
Center	I	15	0.8
Center	V	900	0.8
Center	I	900	0.8
West	V	15	1.0
West	I	15	1.1
West	V	900	1.0
West	I	900	0.9
North	V	15	0.7
North	I	15	0.8
North	V	900	1.0
North	I	900	0.9
East	V	15	0.7
East	I	15	0.7
East	V	900	0.9
East	I	900	0.9
South	V	15	0.8
South	I	15	0.6

3.2. Data reduction and calibration

All the images were pre-processed in the standard way with IRAF, using the sets of bias and sky flat-field images collected during the observing nights. The instrumental magnitudes, and the positions of the stars for each frame were derived by profile-fitting photometry with the package DAOPHOT II and ALLSTAR (Stetson 1987). We then used ALLFRAME (Stetson 1994) to obtain the simultaneous PSF-fitting photometry of all the individual frames. In order to obtain the transformation equations relating the instrumental (vi) magnitudes to the standard V (Johnson), I (Kron-Cousins) system we followed the procedure already described in (Bedin et al. 2000). Seven Landolt (1982) fields of standards were observed. Specifically: the PG0918+029, PG0942-029, PG1047+003, PG1525-071, PG1657+078, SA104334, and SA110-496 regions. In each of these, there are other secondary standard stars by Stetson (2000), which extend the previous Landolt sequence. For all these stars, aperture photometry was obtained on all the images after the digital subtraction of neighboring objects from the frames. We used DAOGROW (Stetson 1990) to obtain the aperture growth curve for each frame and other related codes (by PBS) to determine the aperture corrections, the transformation coefficients, and the final calibrated photometry (e.g., Stetson 1993). We used transformation equations of the form:

$$v = V + A_0 + A_1 * X + A_2 * (V - I),$$

$$i = I + B_0 + B_1 * X + B_2 * (V - I),$$

where the values of the coefficients are listed in Table 3 for the two nights. In these equations v and i are the aperture magnitude already normalized to 1 s, and X is the
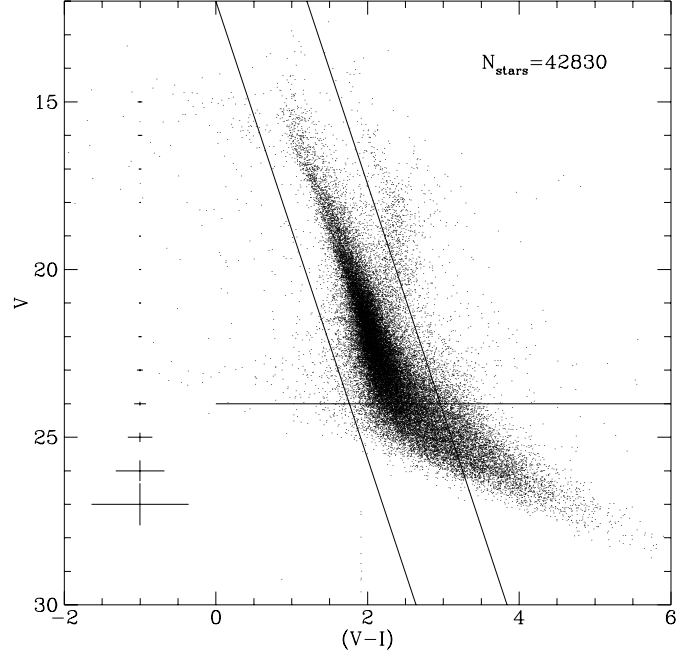

Fig. 1. The CMD of NGC 4815. A selection based on the sharp and chi parameters was done following Stetson (1987). Sharp is vaguely related to the intrinsic (i.e. outside the atmosphere) angular size of the astronomical object. For an isolated star, sharp should have a value close to zero, whereas for semi-resolved galaxies and unrecognized blended doubles sharp will be significantly greater than zero, and for cosmic rays and some image defects will be significantly less than zero. Chi is a robust estimate of the observed pixel-to-pixel scatter from the model image profile divided by the expected pixel-to-pixel scatter from the image profile. The straight lines indicate the CMD region used to derive the LFs and represents the limiting magnitude for the 50% completeness level. Finally, the crosses on the left side of the plot represent the photometric errors at that magnitude level

Table 3. Coefficients of the calibration equations

	April 14, 1999	April 15, 1999
A_0	0.053 ± 0.007	0.044 ± 0.006
A_1	0.249 ± 0.041	0.259 ± 0.023
A_2	-0.036 ± 0.002	-0.028 ± 0.003
B_0	0.690 ± 0.012	0.601 ± 0.012
B_1	-0.054 ± 0.061	0.307 ± 0.050
B_2	0.020 ± 0.002	0.030 ± 0.005

airmass. Second order color terms were tried and turned out to be negligible in comparison to their uncertainties. It is a reasonable hypothesis that the color-dependent terms imposed by the telescope, filter, and detector should be reasonably constant over the course of a few nights, so after A_2 and B_2 were independently determined from each night's data, we obtained weighted mean values of these parameters and imposed them as fixed quantities for the definitive calibration. The NGC 4815 images enabled us to define local standards that met the following conditions: each was well separated from its neighbors (according to a criterion described in Stetson 1993, Sect. 4.1),

each was observed in all frames, each had a mean value of the goodness-of-fit statistic, CHI, less than 1.5. Once calibrated, this local standard sequence enables us to place all of observations of NGC 4815 and of the Galactic fields on the same magnitude system with an uncertainty less than 0.005 magnitudes (internal error).

3.3. Artificial star tests

In order to obtain the LF, we estimated the completeness of our samples. The completeness corrections were determined by standard artificial-star experiments on our data. For each field, we performed five independent experiments adding on the original frames as large a number as possible of artificial stars in a spatial grid, as in (Piotto & Zoccali 1999). We performed the photometry of the frames with the added artificial stars following all the steps and using the same parameters as for the original images. We converted the new instrumental magnitudes to the standard photometric system using the coefficients of the calibration equations of Sect. 2.2.

In the LFs we include only the values for which the completeness corrections, defined as the ratio between the number of found artificial stars to that of the original added ones, were 50% or higher. This sets the limiting magnitude to $V = 24$.

4. The color-magnitude diagrams

We obtained the V and I photometry with the aim of determining the LF (and MF) of the main sequence stars in NGC 4815. We used two colors as we wanted also to derive the CMD, which allows us to: i) discriminate stars from false detections; ii) better identify the cluster population, in particular the MS stars.

The CMD for NGC 4815 is shown in Fig. 1, whereas the CMDs for the four nearby fields are presented in Fig. 2. Clearly, the CMD of the cluster field does not differ much from those of the surrounding Galactic disk. This means that NGC 4815 is actually badly contaminated by background/foreground stars, as expected from its particular position in the Galactic thin disk. The cluster field (Fig. 1) is much more populated than the neighboring fields (Fig. 2), confirming that NGC 4815 is a real open cluster (see also the discussion in Sect. 5). Our photometry reaches $V \approx 25$ at the base of the MS.

The MS extends almost vertically for more than 10 magnitudes, from $V = 15$ to $V = 25$, although the completeness analysis prevents us from using stars dimmer than $V = 24$. The width of the main sequence increases at larger magnitudes. This is partly due to the increasing photometric errors at increasing magnitudes (see Fig. 1). However, the MS is much wider than expected simply from photometric errors. Ways in which the natural MS can be enlarged include the natural MS width we can envisage the presence of unresolved binary stars, common in open clusters, and a possible spread in metals. The red vertical sequence, which detaches from the

MS at about $V = 22.5$ represents the giant branch of the Galactic disk population.

At odds with the previous photometry, the present data (see Fig. 1) do not allow us to recognize clearly the presence of a red giant clump, better visible in the BV photometry of Carraro & Ortolani (1994) at $V \approx 14.3$. This is due to the saturation of many bright stars above $V = 14.5$, which were not of interest to us for the this work.

5. Star counts and cluster size

The aim of this section is to obtain the surface density distribution of NGC 4815, and derive the cluster size and extension in the magnitude space by means of star counts. The cluster radius is indeed one of the most important cluster parameters, useful (together with cluster mass) for the determination of cluster dynamical parameters. Star counts allow us to determine statistical properties of clusters (as visible star condensations) with respect to the surrounding stellar background.

Star counts have been performed following the methods described in Danilov et al. (1986), Seleznev (1994) and Seleznev (1998) by evaluating the functions $N(r)$ and $N(V)$ ($N(I)$). $N(r)$ represents star number in the circle of radius r and $N(V)$ is star number up to apparent magnitude V, i.e. the integral luminosity function. In order to obtain $N(r)$ we divided the cluster field (and comparing fields) in concentric rings 40 pixels (11 arcsec) wide and counted the number of stars falling inside each ring. Then $N(r)$ is obtained by summing the corresponding ring star numbers. Similarly, in order to obtain $N(V)$, we divided stars in the various fields in magnitude bins 0.2^m wide and summed corresponding bin star numbers. Star counts with $N(r)$ give us cluster radius and cluster star number, star counts with $N(V)$ give us the magnitude of the faintest cluster stars (up to the limiting magnitude).

Due to the saturation of the brightest stars ($V < 14.5$), some regions of the cluster cannot be used to perform star counts. In these cases, for $N(r)$ determination we used the stars located in the same regions from the work of Carraro & Ortolani (1994).

A smoothed surface density $F(r)$ is then obtained by numerically differentiating the best fit least squared polynomial approximation for $N(r)$ according to the equation:

$$N(r) = 2\pi \int_0^r r' F(r') \mathrm{d}r' \qquad (1)$$

(see Seleznev 1994, for details). The results are shown in Fig. 3, where the logarithm of the surface density profile is plotted as a function of the limiting magnitude. From this figure it is evident that the cluster significantly emerges from the background only for V less than 21. Below this value, NGC 4815 is completely confused with the Galactic field. Moreover, we note a significant density decrease at the cluster position.
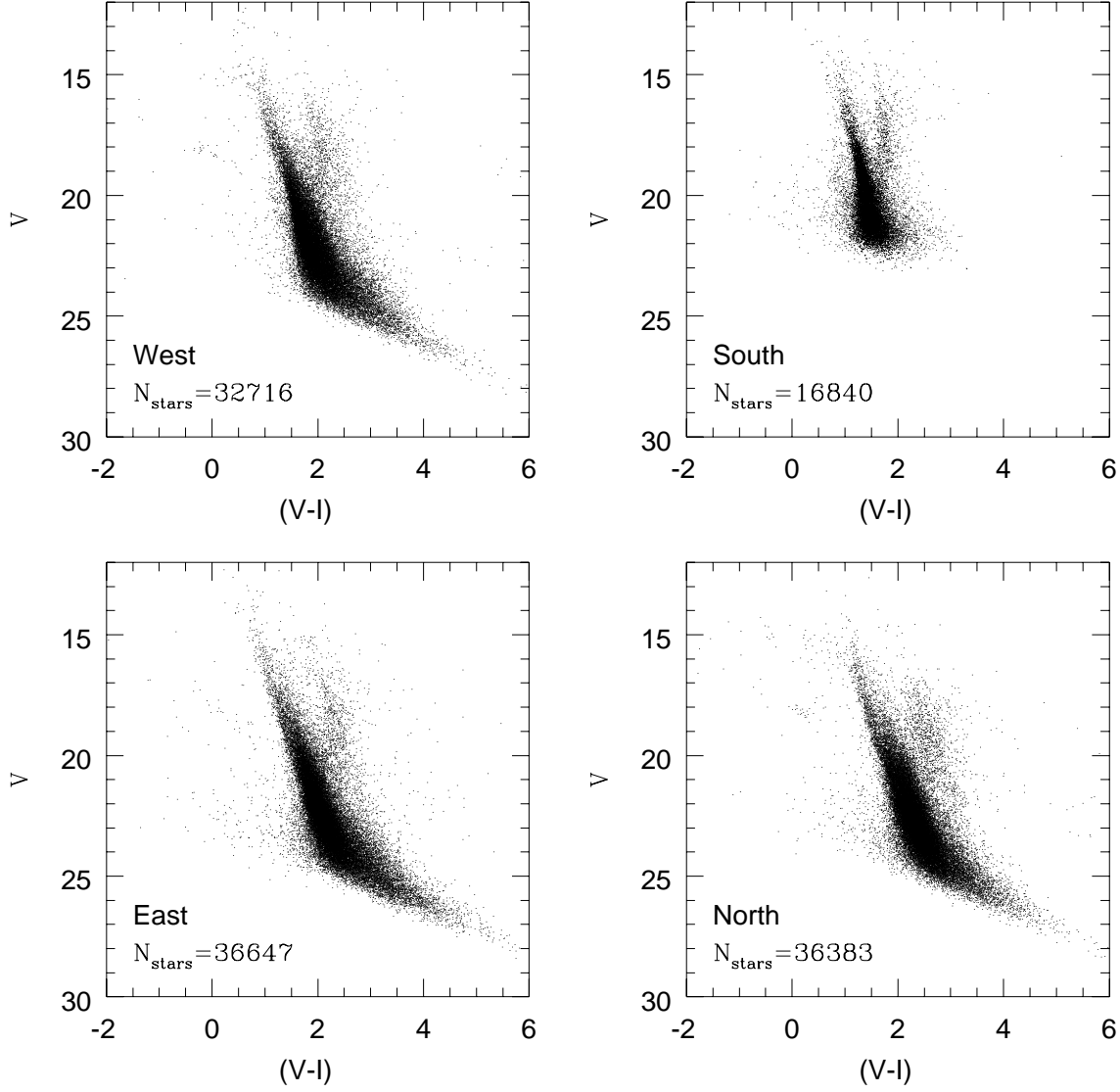
Fig. 2. CMDs of the observed nearby fields. Each field is centered at $30'$ from the center of NGC 4815. The southern field do not have deep exposures, and has not been used in the paper

Integral distribution functions are then obtained both for the cluster field and for comparing fields. Let us consider below a theoretical integral distribution function $N_i(x)$, where x can be r, V and I, and $i = 0$ indicates cluster field, while $i = 1, 2, 3, ...$ indicate comparing fields.

Following Danilov et al. (1986) and Seleznev (1998) we consider the normalized deviation z of $N_i(x)$ from the corresponding average number of field stars:

$$z_i(x) = \frac{\left| N_i(x) - \overline{N(x)} \right|}{\sigma(x)} \qquad (i = 0, 1, \ldots, k), \qquad (2)$$

where

$$\overline{N(x)} = \frac{1}{k} \cdot \sum_{i=1}^{k} N_i(x), \qquad (3)$$

and

$$\sigma^2(x) = \frac{1}{k-1} \cdot \sum_{i=1}^{k} \left[N_i(x) - \overline{N(x)} \right]^2. \qquad (4)$$

The normalized deviations z_i are connected with the probability that the ith field significantly deviates from other fields. Then z values are usually called *significance levels*.

There are two criteria used to determine cluster boundaries in x-space. The first criterion is as follows. One has to look for a value x_c such that $(N_0(x) - \overline{N(x)}) = N_c = $ const. for all $x \geq x_c$ and $z_0(x) \geq z_i(x)$ $(i = 1, 2, 3, ...)$ for all $x \leq x_c$. In this case we can conclude that the cluster has the boundary at the point $x = x_c$ and N_c is the cluster star number, and we can estimate an error for x_c and N_c (Danilov et al. 1986).

The second criterion is as follows. The cluster has no boundary in the sense of the first criterion, but for $x > x_{c2}$ $z_0(x) < z_i(x)$ for some i, i.e. ith field deviates from the mean $\overline{N(x)}$ more significantly than cluster field. This situation means that we can determine only a lower estimate of the cluster boundary, i.e. $x_c > x_{c2}$ and $N_c > N(x_{c2})$. The reason is related to large-scale fluctuations of the integral distribution function in the comparing
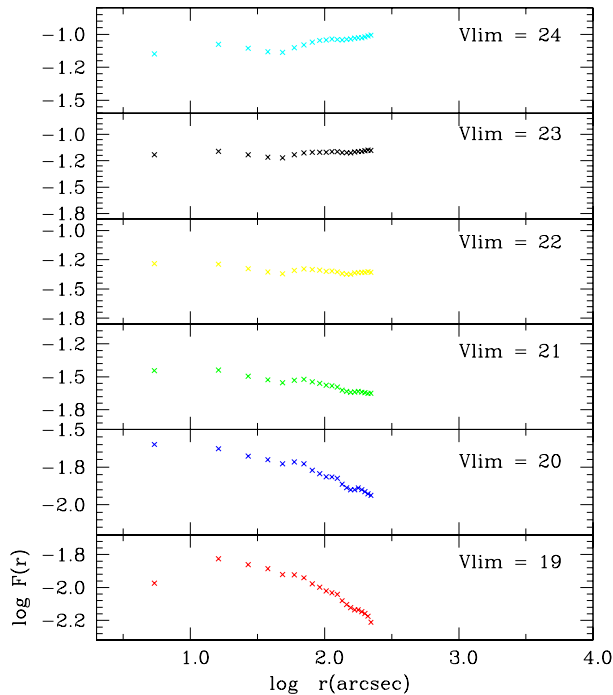
Fig. 3. Radial surface density profiles of NGC 4815 for 6 different limiting magnitudes. Surface density is in stars per arcsec²

Fig. 4. Significance level for cluster and surrounding fields. See text for details

fields. Unfortunately this situation frequently occurs for open star clusters located in a strongly fluctuating background.

The star counts in V and I spaces were performed both for central part of NGC 4815 (circle with $r \approx 2$ arcmin in the central field, see Table 2) with twelve comparing fields (four circles in each East, West and North fields) and for the entire central field with three comparing fields (East, West and North).

The star counts for the central part of the cluster confirm that it is less populated by faint stars ($V > 18^m$–20^m) than the other fields (see Fig. 3). We obtained the cluster boundary $V_c = 20.8^m \pm 0.2^m$ following the first criterion (see above). The trend of $z_0(V)$ is shown in Fig. 4, where it is compared with mean z for North, West and East fields. The luminosity function of cluster stars (see following section), i.e. the differential distribution function, has negative value for $V > V_c$. Presumably, the reason is the higher light absorption along the line of sight beyond the central part of the cluster.

By performing star counts in V and I for all the central field we did not obtain the cluster boundary according to first criterion. In the I passband $N_0(I)$ significantly deviates from mean $\overline{N(I)}$ up to $I \approx 22^m$, but in the V $N_0(V)$ significantly deviates from mean $\overline{N(V)}$ only up to $V \approx 20^m$. However $(N_0(V) - \overline{N(V)})$ and $(N_0(I) - \overline{N(I)})$ increase for much fainter magnitudes, and the corresponding luminosity functions are positive (see Figs. 5 and 6 in the following section). This contradictory result is due to the very complicated character of the stellar background in the vicinity of NGC 4815 and beyond. It means that the mean integral distribution function $\overline{N(V)}$ in the com-
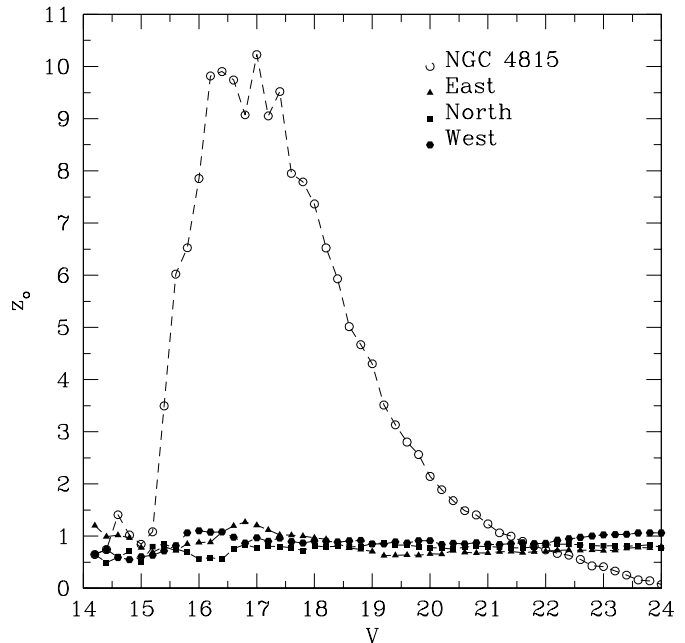
paring fields increases more slowly than $N_0(V)$, but the dispersion $\sigma(V)$ is too large.

Because the cluster center is slightly shifted with respect to the center of the central field, star counts in r-space can be carried out in the entire circle only to radius $r = 880$ pixel (4 arcmin). Due to this, star counts were also made in a sector of 199° to radius $r = 1080$ pixel (4.9 arcmin). The results of star counts for different limiting magnitudes are listed in Table 4.

First column contains the limiting magnitude, the second and third columns contain cluster radius and cluster star number from counts in the entire circle, fourth and fifth columns contain the same values from counts in the 199° sector. Star number in the fifth column is obtained as a result of star counts multiplied by (360/199).

The comparison of results of star counts in the entire circle and in the sector shows that the asymmetry of the cluster increases at increasing limiting magnitude. Beginning from $V_{\mathrm{lim}} = 21^m$ the cluster disappears as a statistically significant stellar density fluctuation, and below $V_{\mathrm{lim}} = 24^m$ the cluster region appears as stellar density minimum – statistically significant when compared with three fields. The most probable reason is the presence of an absorbing cloud just beyond the cluster.

Star counts with stars up to $V_{\mathrm{lim}} = 19^m$ gave us the estimate of cluster radius, which turns out to be 3.6 ± 0.3 arcmin, significantly lower than 4.6 arcmin estimated by Carraro & Ortolani (1994). However, result of Carraro & Ortolani (1994) can be regarded only as preliminary, because cluster radius was determined only by the surface density profile as the distance to a point where the slope of this curve changes, being the slope negative along all the profile. It is difficult to compare our results with previous results directly, because we are now using a

Table 4. Results of star counts for cluster size and star number determination

V_{lim}	Entire circle ($r_{\mathrm{max}} = 880$ pixel)		Sector $199°$ ($r_{\mathrm{max}} = 1080$ pixel)	
	R_{c}	N_{c}	R_{c}	N_{c}
16^{m}	800 ± 71	89 ± 6	800 ± 55	89 ± 2
17^{m}	800 ± 79	219 ± 13	800 ± 40	261 ± 3
18^{m}	800 ± 56	361 ± 11	840 ± 56	454 ± 5
19^{m}	800 ± 64	447 ± 22	> 1080	> 637
20^{m}	> 680	> 319	> 1080	> 599
21^{m}	Cluster does not deviate from comparing fields significantly, $N_{\mathrm{c}} > 0$			
22^{m}	Cluster does not deviate from comparing fields significantly, $N_{\mathrm{c}} < 0$			
23^{m}	Cluster does not deviate from comparing fields significantly, $N_{\mathrm{c}} < 0$			
24^{m}	Cluster significantly deviates from comparing fields as minimum, $N_{\mathrm{c}} < 0$			
24.7^{m}	Cluster significantly deviates from comparing fields as minimum, $N_{\mathrm{c}} < 0$. For $r \in [800, 880]$ $N_{\mathrm{c}} > 0$ and for $r \in [840, 880]$ cluster significantly deviates from comparing fields as maximum.			

quantitative statistical method. Unfortunately, the cluster radius of 3.6 arcmin is very close to the limit of the investigated field, and we can not regard this result as definitive. Furthermore, 3.6 arcmin corresponds to a radius of 2.6 pc at the distance of 2.5 kpc. This value lies in the lower limit of cluster radii interval according to Danilov & Seleznev (1994). It is thus quite possible that we have determined the radius of the cluster core.

It is necessary to note that the central field contains many more stars than any comparing field (see Figs. 1 and 2). This excess in star number is mainly due to the periphery of the central field which is very rich in faint stars. Unfortunately our star counts cannot unambiguously answer the question – is the cluster really disappearing at $V_{\mathrm{lim}} = 21^{\mathrm{m}}$ and does it have a radius of about 3.6 arcmin or do faint stars in the outskirts of central field belong to the cluster and form its halo?

Firstly, star counts in wider fields are necessary (both for cluster and comparing fields). A desirable radius for the investigated field is about 10–15 pc (i.e. 14–21 arcmin). Secondly, it is necessary to study color extinction for stars of different magnitudes, i.e. to observe in three colors. On the basis of the previous discussion, we are going to estimate the luminosity function for the central field in the magnitude range $V \in [14^{\mathrm{m}}; 24^{\mathrm{m}}]$.

6. Luminosity function

The luminosity function of NGC 4815 was obtained as follows. In the CMDs, two lines, to the left and right of the main sequence, defined by the two relations $V = 6.8(V - I) + 12$ and $V = 6.8(V - I) + 3.84$, were used to select only the main sequence stars (Fig. 1). For each field, an adaptive kernel estimator was then applied to obtain a continuous LF. The LF was also derived by the standard histogram technique. A detailed description of the application of the kernel function method for estimating distribution functions can be found in Silverman (1986), and in Seleznev (1998) and Seleznev (2000).

The advantage of this method is twofold: 1) it is not necessary to define a bin, whose size usually is arbitrary and does not allow us to detect unambiguously all the statistically significant features present in the LF; the estimate of the LF by a kernel method with its confidence interval is an estimate of an unknown density of a stellar population, while the histogram alone gives only the distribution of a specific sample; 2) the form of a histogram – crucial for the determination of the LF slope – depends both on the bin width and on the initial bin location. The distribution function provided by the kernel estimate only depends on the kernel width. Moreover criteria were developed to fix the kernel width with a high degree of confidence (Silverman 1986).

The adaptive kernel estimate of the density distribution in one-dimensional case is calculated by the formula:

$$\hat{f}(x) = \frac{1}{n} \sum_{i=1}^{n} h\lambda_i \cdot K\left(\frac{x - X_i}{h\lambda_i}\right), \qquad (5)$$

where n is the size of the observing sample $X_1...X_n$ of the random variable x, K is the kernel function which must satisfy the condition:

$$\int_{-\infty}^{+\infty} K(x)\mathrm{d}x = 1, \qquad (6)$$

and λ_i are the local window width factors. The adopted kernel has the form

$$K(x) = \frac{3}{4\sqrt{5}}\left(1 - \frac{x^2}{5}\right) \qquad (7)$$

when $|x| \leq \sqrt{5}$, and zero elsewhere.

Basically Eq. (5) spreads each observed value X_i of the random variable x over an interval (window) centered on X_i with the probability density $K\left(\frac{x-X_i}{h\lambda_i}\right)$. The kernel width $h\lambda_i$ can differ from point to point. The advantage of having an adaptive kernel is that it is easy to properly sample the tails of the distribution, just playing with the
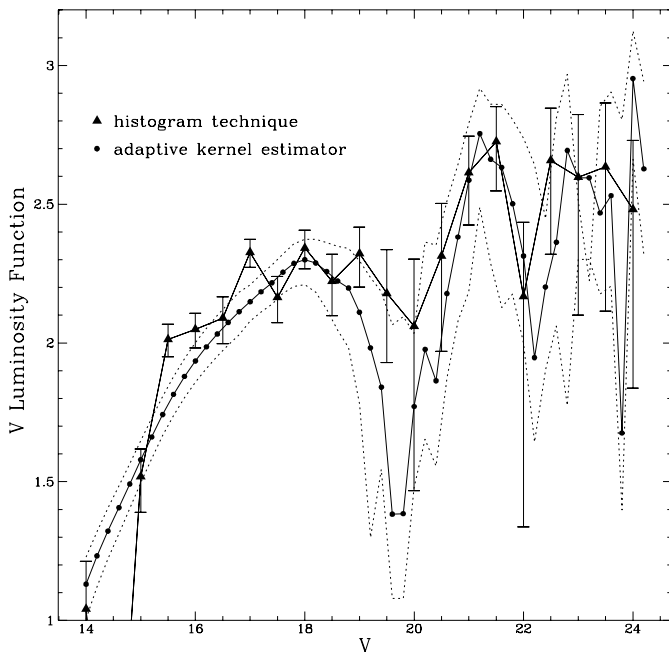
Fig. 5. The V LFs obtained with both the standard histogram technique (*triangles*) and with an adaptive kernel estimator (*circles*). The *dotted curves* are the confidence intervals for the adaptive kernel estimator. Note the large error bars below $V = 21$, when the clusters starts to vanish into the Galactic field
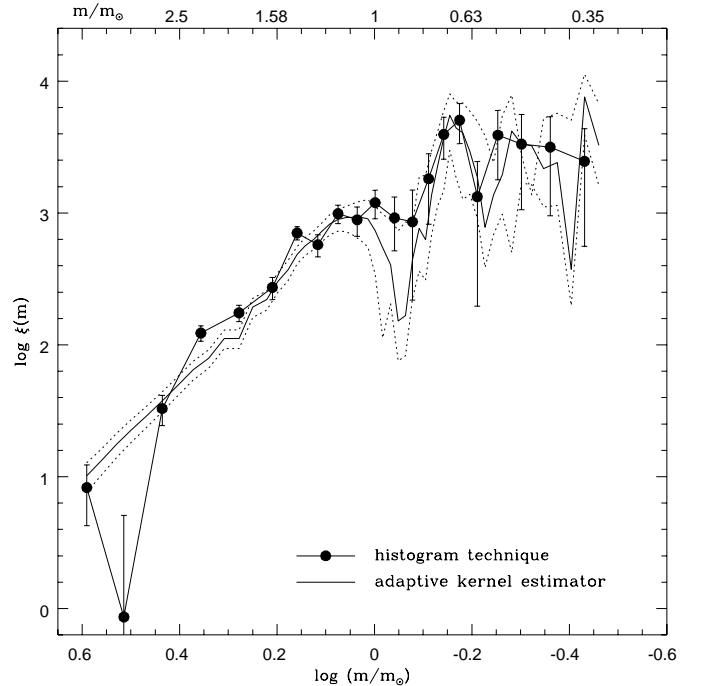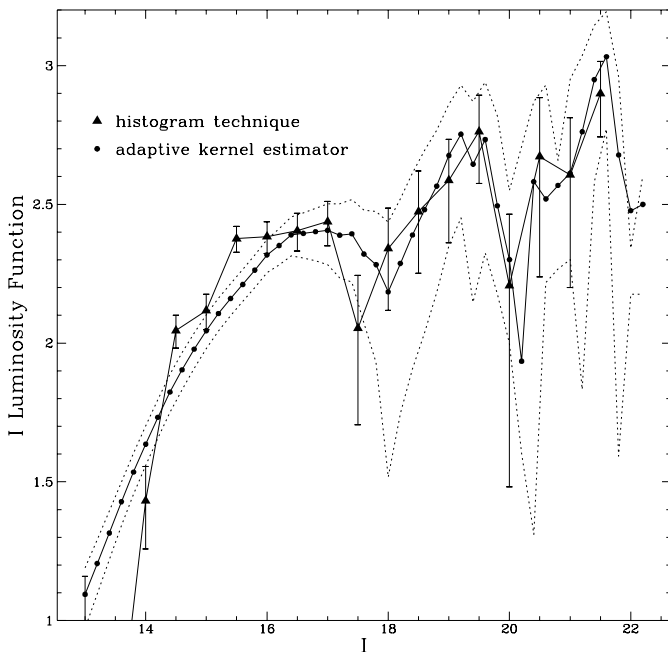

Fig. 6. As for Fig. 5, but for the I filter

kernel width, which is set larger in low-density regions automatically (see Silverman 1986). Parameter h was set to be 0.3^{m}.

To determine the confidence interval for the resulting LF, we used the method described in Seleznev et al. (2000) and references therein.

Fig. 7. Comparison of the MFs of NGC 4815 from V LFs derived by the adaptive kernel estimator and the standard histogram technique. The *dotted curves* are the confidence intervals for the adaptive kernel estimator

For each field, the LFs were corrected for incompleteness. The LFs of the external fields were used to subtract the field-star contamination from the LF of the central field.

To this end we defined $\hat{f}_i(V)$ as the density of the distribution of the stellar V magnitudes, where i is the number of the field (here we assume that $i = 0$ corresponds to the cluster field or central field and $i = 1, 2, 3$ correspond to the external fields). The luminosity function of the cluster stars is given by

$$\hat{f}(V) = \hat{f}_0(V) - \frac{1}{k} \sum_{i=1}^{k} \hat{f}_i(V). \tag{8}$$

The same procedure was repeated to get the I LF. The V and I LFs obtained both with the histogram and the adaptive kernel techniques for all the central field are shown in Figs. 5 and 6. Note the large uncertainties below $V = 21$ ($I \sim 19$), where fluctuations of stellar background density play a significant role. LFs obtained by different methods are close each other due to large volume of the sample. Note that the stellar content below $V = 20$ ($I = 18$) is due to the outskirts of the central field (see previous section).

7. Mass function

The LFs can be transformed into MFs using a mass-luminosity relation (MLR). Since we cannot obtain an empirical transformation, we must rely on the theoretical models. Therefore, we used the ZAMS isochrones by
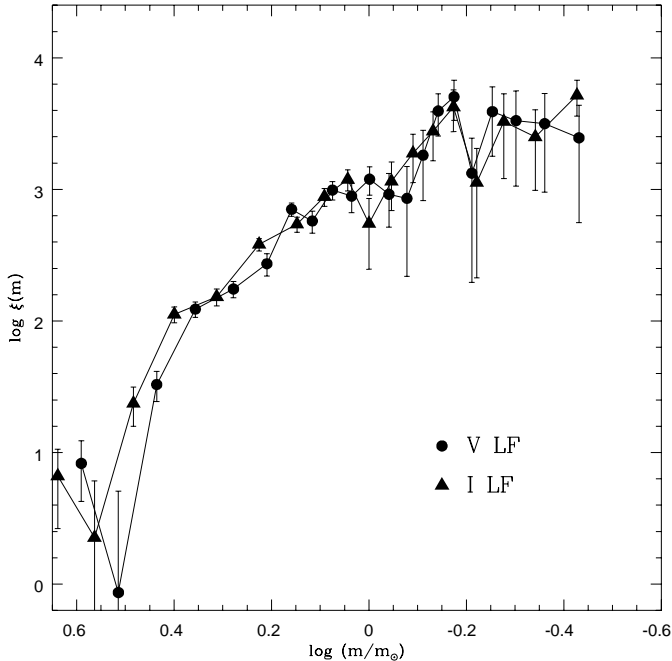
Fig. 8. Comparison of the MFs of NGC 4815 from the V and I LFs derived by the standard histogram technique
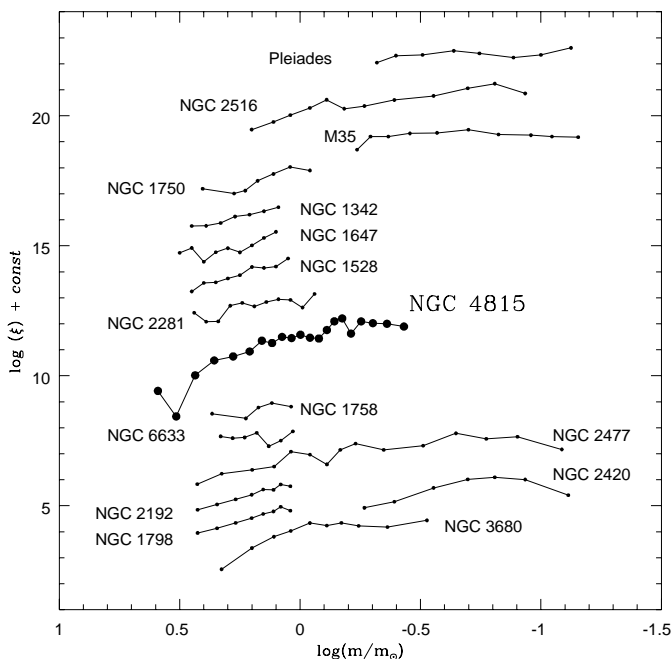

Fig. 9. Comparison of the NGC 4815 MF with other open cluster MFs. For display purposes the MFs are shifted by an arbitrary constant

Girardi et al. (2000) with a metallicity $Z = 0.008$. The distance modulus and the reddening that result from the fit with the model are in agreement, within the errors, with the values found by Carraro & Ortolani (1994). We adopted $E(B - V) = 0.70$ and $(m - M)_V = 14.10$. From these values we get $(m - M)_I = 13.20$ (see Table 1). Figure 7 shows the MF from the V LFs obtained by the adaptive kernel estimator and the standard histogram

technique. The two MFs are rather similar. There is also a substantial agreement between the MFs from the V and I LFs (Fig. 8), showing an internal consistency of both the models and the method.

By looking at Fig. 7, it appears that there is a dip in MF at $m \simeq 0.9\ M$. This dip in MF is a consequence of the corresponding dips in LFs at $V \simeq 19.5^{\mathrm{m}}$–$20^{\mathrm{m}}$ and $I \simeq 17.5^{\mathrm{m}}$–$18^{\mathrm{m}}$ (see Figs. 5 and 6). To estimate the statistical signifincance of this dip, we concentrate on *Adaptive Kernel Estimator* method, which is more sensitive to peculiar properties of LF and MF than the histogram technique (see previous sections).

We can use the ratio η of the depth of this minimum (relatively to the mean smooth MF level) to the dispersion of the MF estimate in the vicinity of the MF minimum as a measure of the statistical significance of the MF minimum. As for the MF minimum at $m \simeq 0.9\ M$. we obtain $\eta \simeq 1.98$ from the *adaptive kernel* MF estimate, which corresponds to a reality probability of $\sim 95\%$. On the other hand, $\eta \simeq 0.78$ comes out of the *histogram* MF estimate, which corresponds to probability of $\sim 56\%$. We can thus conclude that this dip of MF seems to be statistically significant.

Finally, it is possible to obtain an estimate of the cluster mass by integrating the luminosity function. In detail,

$$M = <m> \times N = N \int_{M_{V_{\mathrm{min}}}}^{M_{V_{\mathrm{max}}}} m(M_V)\phi(M_V)\mathrm{d}M_V \qquad (9)$$

where M_V is absolute stellar magnitude $M_V = V - (m - M)_V$, $\phi(M_V)$ is the normalized luminosity function

$$\phi(M_V) = f(M_V)/N, \qquad (10)$$

N is the total number of stars, $m(M_V)$ is the adopted mass-luminosity relation. The luminosity function and mass-luminosity relation have been approximated by a spline. Limits in the integral are $M_{V_{\mathrm{min}}} = -0.1$ and $M_{V_{\mathrm{max}}} = 9.9$. The integral turns out to be

$$M \simeq 1620 \pm 690\ M_\odot$$

for kernel LF estimate and

$$M \simeq 1820 \pm 650\ M_\odot$$

for histogram LF estimate.

This mass estimate refers to the total central field. Unfortunately it is very difficult to evaluate what part of the total cluster mass is constituted by this estimate. It depends on both the unknown cluster size and the unknown upper limit of magnitude. If we assume that NGC 4815 has a limiting magnitude of $V_{\mathrm{c}} = 20.8^{\mathrm{m}}$, we get the mass estimate

$$M \simeq 880 \pm 230\ M_\odot.$$

The error is determined from mass estimate for upper and lower boundaries of the confidence interval for LF (see Fig. 5).

8. Discussion and conclusions

The MF cannot be represented by a unique power law. In the mass range $2.5 < m/m_\odot < 0.8$, the PDMF is reproduced by a power-law with $\alpha = 3.1 \pm 0.3$ ($\alpha = 2.35$ for the Salpeter MF in this notation). In the same mass range, the slope of the MF from the I LF is $\alpha = 2.9 \pm 0.3$.

Below 0.8 $m_\odot$, the MF is much flatter ($\alpha = -0.68 \pm 0.49$).

It is difficult to correctly interpret the PDMF in this low mass regime. However we believe that the flattening of the PDMF below 0.8 $m_\odot$ can be due to basically two effects.

First, we have already noted how the cluster vanishes (but does not disappear) into the Galactic field below $V = 21$, i.e. $m = 0.8\ m_\odot$. This is likely caused by irregularities in the stellar background. As a consequence, low mass stars are preferentially missed due to absorption.

Secondly, we cannot exclude cluster dynamical evolution, which preferentially causes a loss of low mass stars. Also, stripping of low mass stars can occur along the cluster orbit, due to the interaction of the cluster with the dense Galactic field. NGC 4815 is indeed located close to the Sagittarius-Carina spiral arm, rich in HII regions and molecular clouds. Estimating the relative importance of these two effects is very difficult and goes beyond the aim of this paper.

Therefore, the slope of the MF below 0.8 $m_\odot$ cannot be considered representative of the cluster IMF.

On the other hand, whether the PDMF above 0.8 $m_\odot$ is representative of the IMF is also a matter which requires a careful model of the cluster.

A recent review of the IMF derived from the star counts is given in Scalo (1998). From the comparison of several studies, he found that the spread in the slope at all masses above about 1 $m_\odot$ is too large to adoptsome average value, and in particular, there is no evidence for a clustering of points around the Salpeter value (2.35). Scalo (1998) concluded that either the systematic uncertainties are so large that the IMF cannot yet be estimated, or that there are real and significant variations of the IMF slope. Clearly, the dynamical evolution, which differs from cluster to cluster, can modify the MF slope, and this effect also contributes to the MF slope dispersion. It has emerged that the MF cannot be reproduced with a single power law: at low-masses the IMF from the field stars, open and globular clusters is relatively flat, and it becomes steeper above about 1 $m_\odot$. NGC 4815 seems to show this break in the MF shape at $m \sim 1\ m_\odot$ (Fig. 7), though it is not possible to disentangle the real differences in the IMF from the effects of the dynamical evolution. A final point is the effect of unresolved binaries and mass segregation. As discussed by Scalo (1998, and references therein), unresolved binaries and mass segregation can only flatten the apparent IMF derived by not accounting for these, so the real IMF must be steeper than the quoted slope by an unknown amount.
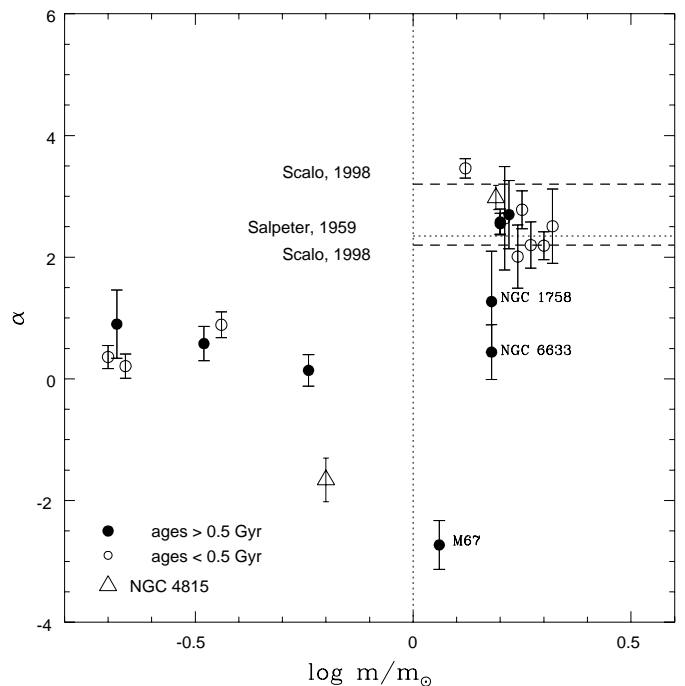

Fig. 10. The MF slopes α are plotted as a function of the mean fitting mass in the two mass ranges: $m > 1\ m_\odot$ and $m < 1\ m_\odot$. Filled circles represent clusters older than 0.5 Gyr, whereas open cirles stand for younger clusters. Note the similarity of the MF slopes for the youngest clusters

In Fig. 9, the MF of NGC 4815 is compared with the MFs for 15 other open clusters. Most of them cover masses above 1 $m_\odot$. We have derived the MFs directly from the published LFs using the same set of isochrones from Girardi et al. (2000) used to get the NGC 4815 MF. The MFs in Fig. 9 are shifted by arbitrary constants for display purposes. The MF of NGC 4815 is one of the most extended (in mass) MFs obtained so far for an open cluster. Only for the better known and nearby open clusters (Pleiades and M 35), and for objects observed with HST (NGC 2516, NGC 2477, and NGC 2420) do the MFs reach $\simeq 0.1\ m_\odot$.

Figure 10 shows the slopes α of the MFs plotted in Fig. 9 as a function of the mean mass. The slopes have been obtained by fitting a power law in the $m < 1\ m_\odot$ and $m > 1\ m_\odot$ mass ranges. Clusters with ages greater and less than or equal to 0.5 Gyr are plotted with different symbols. As noted by Scalo, the spread in slope is very large. However, it is interesting to note that *all* the clusters with ages ≤ 0.5 Gyr have very similar slopes ($\alpha = 2.25 \pm 0.88$) for $m > 1 m_\odot$.

NGC 4815, which has an age of 0.5 Gyr (Carraro & Ortolani 1994), has a MF slope fully consistent with this value. The MFs of the clusters older than 0.5 Gyr have a similar or flatter slope. This indicates that their PDMF may have beenchanged by the dynamical evolution which has had more time to operate. A dynamical model of each of these clusters is necessary to confirm this interpretation of Fig. 10. At the moment, the similarity of the MF

slopes for all the youngest clusters in Fig. 10 can be interpreted as evidence for a similarity of the IMF, which seems not to depend much on metallicity, stellar density, or galactocentric radius.

The interpretation of the MF slopes below 0.8 $m_\odot$ is more difficult, both because there is less (and more uncertain) data, and because we expect that in this mass regime the dynamical evolution should be more effective in altering the IMF. Still, all the MFs seems to have the same general flat trend. We also note that these slopes represent an upper limit for the slopes of the MF of the Galactic globular clusters (Piotto & Zoccali 1999).

References

Aarseth, S. 1996, 423
Bedin, L., Piotto, G., Zoccali, M., et al. 2000, A&A, 363, 159
Carraro, G., & Ortolani, S. 1994, A&AS, 106, 573
Chen, B., Carraro, G., Torra, J., & Jordi, C. 1998, A&A, 331, 916
Danilov, V. M., Matkin, N. V., & Pyl'skaja, O. P. 1986, Astr. Zhurn, 62, 1065
de la Fuente Marcos, R. 1997
Friel, E. D. 1995, ARA&A, 33, 381
Girardi, L., Bressan, A., Bertelli, G., & Chiosi, C. 2000, A&AS, 141, 371
Janes, K., & Adler, D. 1982, ApJS, 49, 425
Kjeldsen, H., & Frandsen, S. 1991, A&AS, 87, 119
Moffat, A. F. J., & Vogt, N. 1973, A&AS, 10, 135
Piotto, G., & Zoccali, M. 1999, A&A, 345, 485
Salpeter, E. E. 1955, ApJ, 129, 608
Scalo, J. 1998, in ASP Conf. Ser. 142, The Stellar Initial Mass Function, 38th Herstmonceux Conference, 201+
Seleznev, A. F. 1994, Astron. Astrophys. Trans., 4, 167
Seleznev, A. F. 1998, Astron. Rep., 42, 153
Seleznev, A. F., Carraro, G., Piotto, G., & Rosenberg, A. 2000, Astron. Rep., 44
Silverman, B. W. 1986, Density estimation for statistics and data analysis, Monographs on Statistics and Applied Probability (London: Chapman and Hall), 1
Stetson, P. B. 1987, PASP, 99, 191
Stetson, P. B. 1990, PASP, 102, 932
Stetson, P. B. 1993, IAU Colloq., 136, 291
Stetson, P. B. 1994, PASP, 106, 250
Stetson, P. B. 2000, PASP, 112, 925
Terlevich, E. 1987, MNRAS, 224, 193
Theuns, T. 1992a, A&A, 259, 493
Theuns, T. 1992b, A&A, 259, 503
van den Bergh, S., & McClure, R. D. 1980, A&A, 88, 360
Wielen, R. 1971, A&A, 13, 309